Top electrode size effect on hysteresis loops in piezoresponse force microscopy of $Pb(Zr,Ti)O_3$-film on silicon structures

Cite as: J. Appl. Phys. **112**, 052015 (2012); https://doi.org/10.1063/1.4746028
Submitted: 02 December 2011 • Accepted: 30 April 2012 • Published Online: 04 September 2012

S. L. Bravina, N. V. Morozovsky, E. A. Eliseev, et al.

Top electrode size effect on hysteresis loops in piezoresponse force microscopy of $Pb(Zr,Ti)O_3$-film on silicon structures

S. L. Bravina,[1,2] N. V. Morozovsky,[1,2] E. A. Eliseev,[1] A. N. Morozovska,[1] J. Costecalde,[2] C. Soyer,[2] D. Remiens,[2] and D. Deresmes[2]
[1]*Institute of Physics of National Academy of Science of Ukraine, 46, Prospect Nauki, Kiev 03028, Ukraine*
[2]*IEMN-DOAE-MIMM Team, CNRS UMR 8520, Bat. P3, Cité Scientifique USTL, 59652, France*

(Received 2 December 2011; accepted 30 April 2012; published online 4 September 2012)

Experimental and theoretical studies of hysteresis loops in piezoresponse force microscopy (PFM) directed on elucidating the influence of top electrode lateral sizes on loop peculiarities were performed for $Pt/Pb(Zr, Ti)O_3/Pt/TiO_x/SiO_2/Si$-substrate structures. The set of top Pt electrodes (50 nm to 10 μm of lateral size) was deposited on the $Pb(Zr_xTi_{1-x})O_3$ film ($x = 0.54$, thickness ≈ 1 μm) by RF magnetron sputtering. Under approaching the top electrode lateral size to the film thickness, the transition-like behaviour of PFM response amplitude and coercive tip voltage was observed. The existence of the critical value of dimensionless electrode size parameter $\gamma d/h \approx 1$ (γ is the dielectric anisotropy factor, d is the electrode size parameter, and h is the film thickness) was interpreted in the framework of the model based on Landau-Ginzburg-Devonshire theory combined with the decoupling approximation subject to the nonlinear electric field dependence of the ferroelectric polarization and dielectric permittivity. © *2012 American Institute of Physics*. [http://dx.doi.org/10.1063/1.4746028]

I. INTRODUCTION

Piezoelectric micro- and nano-structures based on lead zirconate-titanate, $Pb(Zr_xTi_{1-x})O_3$ (PZT), films on silicon structures are widely studied for creating micro/nano-electromechanical systems ((M/N)EMS)[1] and cells of ferroelectric non-volatile random access memories (FeRAMs).[2] The electromechanical characterization of these systems by double-beam laser interferometry[3] demonstrated the top electrode size influence on the effective piezoelectric coefficient $d_{33}{}^{,\mathrm{eff}}$.[4] It was reported that $d_{33}{}^{,\mathrm{eff}}$ value decreased with decreasing size of Pt top electrodes for the electrode lateral sizes of 5 mm to 100 μm. This electrode size effect as well as extremely increased piezoelectric parameters measured by charge integration[5] was ascribed to the measurement method features. These results demonstrate the necessity of taking into account the measurement conditions when interpreting experimental data.

Since development of sub-micron and nano-sized ferroelectric film structure technologies and appropriate nanoscale techniques, in particular atomic force microscopy (AFM),[6] much attention has been paid on studying various size effects observed under examining these structures. In particular, intensive studies of polarization reversal characteristics of ferroelectric film structures for (M/N)EMS and FeRAMs applications revealed a set of size effects that are specified not only by fundamental aspects of the kinetics and thermodynamics of nucleation and domain wall motion but also by technology of structure formation and measurement techniques.

Extensive application of piezoresponse force microscopy (PFM) for imaging ferroelectric domain structures and domain engineering requires clarifying sources of size effects connected with interaction between a force microscope tip and ferroelectric domains.[7–16] In particular, PFM response hysteresis loop formation is currently studied with special emphasis on the tip size effect on a local piezoelectric response.[17,18] It was shown[17] that an effective PFM response value is independent on a tip radius until the electric voltage applied to the tip is small in comparison with the coercive one. Recently, the finite size effects in the PFM response hysteresis loop originating from the interplay between the tip radius and film thickness have been studied theoretically[18] and the top electrode size influence on the PFM loop parameters was found for ferroelectric PZT films.[19]

In this paper, we present the results of experimental and theoretical studies of electrode size effect in PFM response of PZT film structures with the set of micro- and nanometrically scaled top electrodes in order to elucidate the influence of top electrode lateral sizes on PFM response amplitude and phase loops and coercive voltage values.

II. EXPERIMENTAL

A. Structure preparation

PZT film of investigated $Pt/PZT/Pt/TiO_x/SiO_2/Si$ structure was prepared by the radio-frequency magnetron sputtering method. The bottom Pt electrode of 150 nm of thickness was deposited on the 350 nm SiO_2 layer on 350 μm (100) n-type Si wafer. The $Pb(Zr_xTi_{1-x})O_3$ film ($x = 0.54, \approx 1$ μm thickness) was deposited on the $Pt/TiO_x/SiO_2/Si$-substrate structure just after its stabilization by annealing treatment at 650-700 °C. The set of evaporated top Pt (50 nm) electrodes with lateral size from 50 nm to 10 μm were obtained on the same PZT film by classical lift-off technique using PMMA resist. At that, the following technology steps were performed: (a) PMMA (4% 950 K) monolayer (180.8 nm) deposition; (b) deposition of 5 nm Ge layer for charge removing; (c) electron beam lithography of PMMA; (d) Ge layer

removing with H_2O_2/H_2O and electrode place preparation with methyl isobutyl ketone and alcohol isopropylene; (e) Pt deposition by vacuum evaporation; (f) PMMA extraction by lift-off in Remover PG at 80 °C under stirring.

The perovskite ferroelectric phase of PZT was obtained by annealing the structure at 625°C for 30 min. The sputtering conditions and the results of x-ray diffraction characterization of PZT film microstructure were described in detail in Refs. 20 and 21.

XRD patterns[20] evidenced the perfect crystallization in the perovskite phase without pyroclore phase inclusions. The films are polycrystalline with (101)/(110) or (111)—preferred orientation for all film thickness in the range 0.1–3 μm. The investigated films of about 1 μm thickness consists of grains with preferred (101)/(110) orientation and lateral sizes of about 1 μm. The results of studies of macroscopic piezoelectric, ferroelectric, and pyroelectric properties of these films were reported earlier.[20,22,23]

B. Measurements

AFM and PFM observations were performed with a Veeco "Dimension 3100" microscope using the same probe of *App-Nano* ANSCM-PA type with the cantilever spring constant of ≈40 N/m (resonance frequency 300 kHz). The probe was equipped by Si tip with apex radius less than 10 nm and double layer of chromium and platinum/iridium5 (Pt/Ir5) coating of 23 nm thick on both sides of the probe resulting in tip curvature radius ≈30 nm.

The AFM topography images were obtained in the tapping mode. After localization of the top Pt electrode by AFM imaging, the PFM response measurements were carried out by switching the microscope in contact mode. A modulation ac voltage of 2 kHz frequency and 1.5 V of amplitude was applied to the conductive PFM tip and dc driving voltage V_d cycled in the range $-10\ V \le V_d \le +10\ V$ was applied to the bottom Pt electrode of the film. The amplitude of V_d was chosen to be higher than the coercive voltage for polarization reversal in the examined PZT film. PFM response amplitude and phase hysteresis loops were recorded as a function of V_d by demodulating photoelectrically transformed cantilever deflection signal with a lock-in amplifier Signal Recovery 7270.

Figure 1 presents AFM topography images of PZT film surface with 10 μm (Fig. 1(a)) and 100 nm (Fig. 1(b)) sized Pt/Ti top electrodes and also the examples of electrode topography (Figs. 1(c) and 1(d)). The seeming large scale of 100 nm electrode topography (≈150 nm) (Fig. 1(d)) can be connected with the proximity of electrode size and used tip diameter (≈60 nm).

Figure 2 presents the AFM topography and PFM response images of 1 × 1 μm fragment of a free film surface. AFM topography images (Figs. 2(a) and 2(b)) display a well distinguished inter-grain boundary and two grains with well developed amplitude and phase surface patterns.

PFM amplitude and phase images of as prepared film (Figs. 2(c) and 2(d)) show similar PFM amplitude patterns for the grains and the same phase of local electromechanical response of the grains with gradation between bright and dark, which corresponds to different polarization values but with the same out-of-plane polarization direction (except some defect regions).

PFM amplitude image of the film poled at 5 V (Fig. 2(e)) shows more uniform amplitude distribution inside each grain and different polarization values in the adjacent grains. PFM phase image (Fig. 2(f)) indicates the same phase of electromechanical response for the grains that correspond to the same out-of-plane polarization direction.

In general, the PFM amplitude and phase images show no regular domain structure similar to those observed in epitaxial PZT films.[39] For the investigated polycrystalline granular PZT films[20] such PFM image is typical and similar to that reported, for example, for granular $PbTiO_3$:La films.[24]

For micro-scaled electrodes (1-10 μm), the PFM measurements were performed with PFM tip located over the PZT grain (1-3 μm) distinguished through the top Pt electrode. For

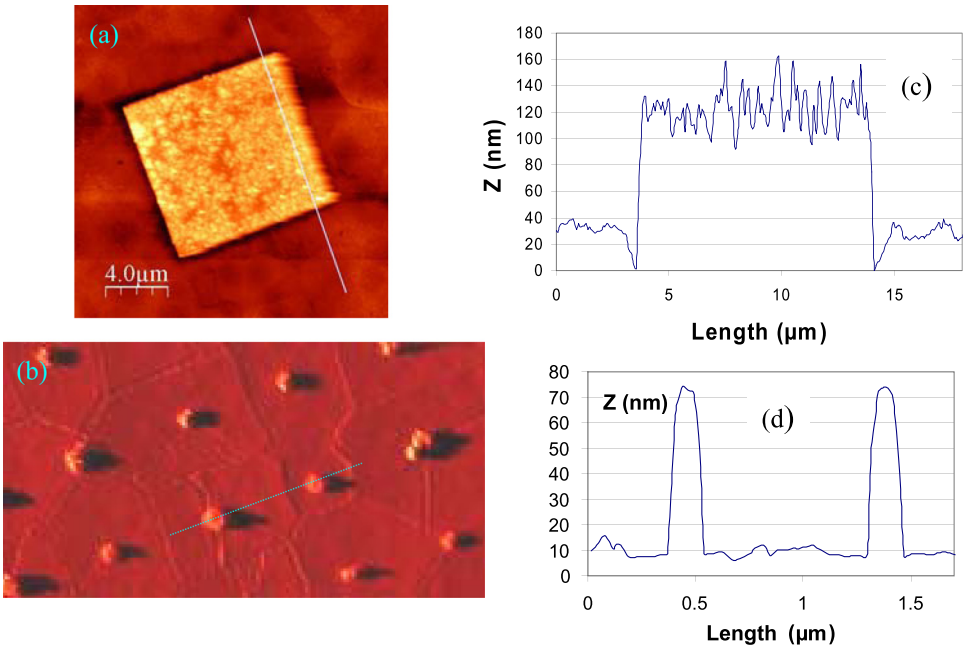

FIG. 1. AFM topography images of PZT film surface: (a) with 10 μm sized Pt/Ti top electrode; (b) with 1 μm ranged 100 nm sized Pt/Ti top electrodes; (c) and (d) topographies along scanning run indicated in (a) and (b) by light blue lines.

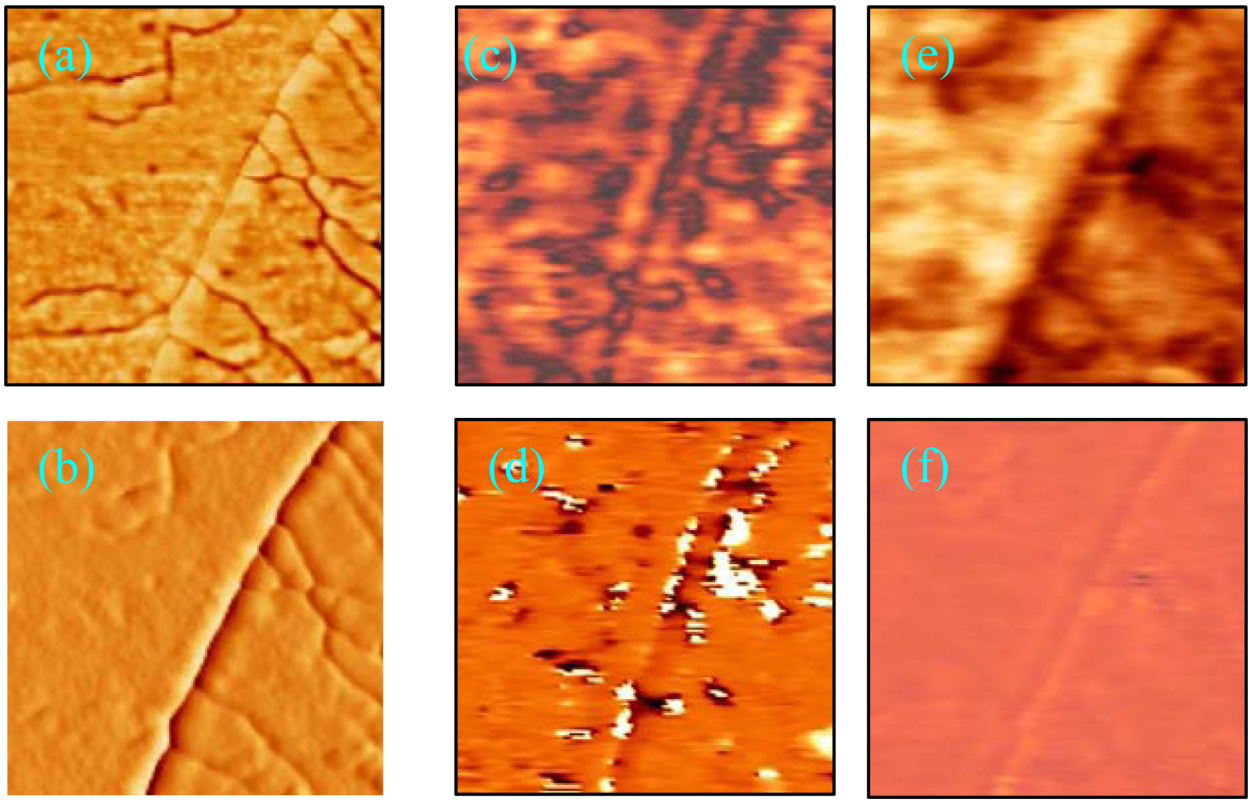

FIG. 2. AFM topography (a) and (b) and PFM-response (c)–(f) 1×1 μm images of PZT film surface with adjacent grain regions. (a), (c), and (e) Amplitudes; (b), (d), and (f) phases of an as prepared ((c) and (d)) and ((e) and (f)) poled at 5 V film.

nano- and meso-scaled electrodes (50-500 nm), the PFM measurements were performed on the electrodes located on the grains far from the grain boundaries selected under operation in AFM topography and PFM image modes.

C. Results and comments

The obtained PFM response amplitude and phase loops of PZT films with micro- and nanometrically sized top electrodes are presented in Figure 3. The PFM response amplitude loops (Fig. 3, left) possess butterfly-like shape with saturated wings and zero deformation when driving voltage V_d achieves the value of the coercive tip voltage V_{tc}. The PFM response phase loops (Fig. 3, right) are of near rectangular shape with near 180°-jumps at $V_d = V_{tc}$, which reflect the change of the sign of deformation under polarization reversal in the film.

In the phase loops, "spike-like" and other pulsed irregularities of different intensity and shape are often observed in V_{tc} vicinities just before and just after polarization reversal and correspond PFM signal phase glitch at the moment of quick change of sign of measured piezoelectric reaction.

The effect of significant change of PFM loop parameters under decreasing the top electrode lateral size is clearly demonstrated in the behaviour of coercive tip voltages V_{tc}^{+} and V_{tc}^{-} and the PFM response amplitudes A_m^{+} and A_m^{-} (indices "+" and "−" correspond to positive and negative PFM response loop branches). In fact, the values of $V_{tc}^{+/-}$ and $A_m^{+/-}$ decrease considerably under electrode sizes decreasing lower than the film thickness ≈ 1 μm (Fig. 3, left). At that point, the narrowing of the PFM response phase loops corresponds to the same tendency in the behaviour of amplitude loops (Fig. 3, right).

This transition-like electrode size effect of decreasing the PFM response loop main parameters under decreasing the top electrode dimension relative to the film thickness can be connected to the transition from the operation in the quasi-uniform electric field realized for micro-sized electrodes (a planar top-bottom electrode system) to the operation in the non-uniform electric field realized for nano-sized electrodes (a point top–planar bottom electrode system) under top electrode size decreasing.[25]

III. THEORETICAL MODEL

Recently,[18] Landau-Ginzburg-Devonshire (LGD) theory was combined with decoupling approximation,[17,26,27] in order to interpret the tip size effect in PFM response hysteresis loop formation. In contrast to the "rigid" approximation previously used for analysis of PFM loops,[28] the combined approach allows calculations of the local piezoelectric response loop parameters, in particular coercive voltages, taking into account the nonlinear field dependence of the ferroelectric polarization and dielectric permittivity during the local polarization reversal.[18]

Such theoretical consideration can be directly applied to the obtained experimental results on top electrode size effect in PFM response of the studied PFM ⟨⟨tip—top electrode/PZT film/bottom electrode⟩⟩ system with the set of micro- and nano- scaled top electrodes.

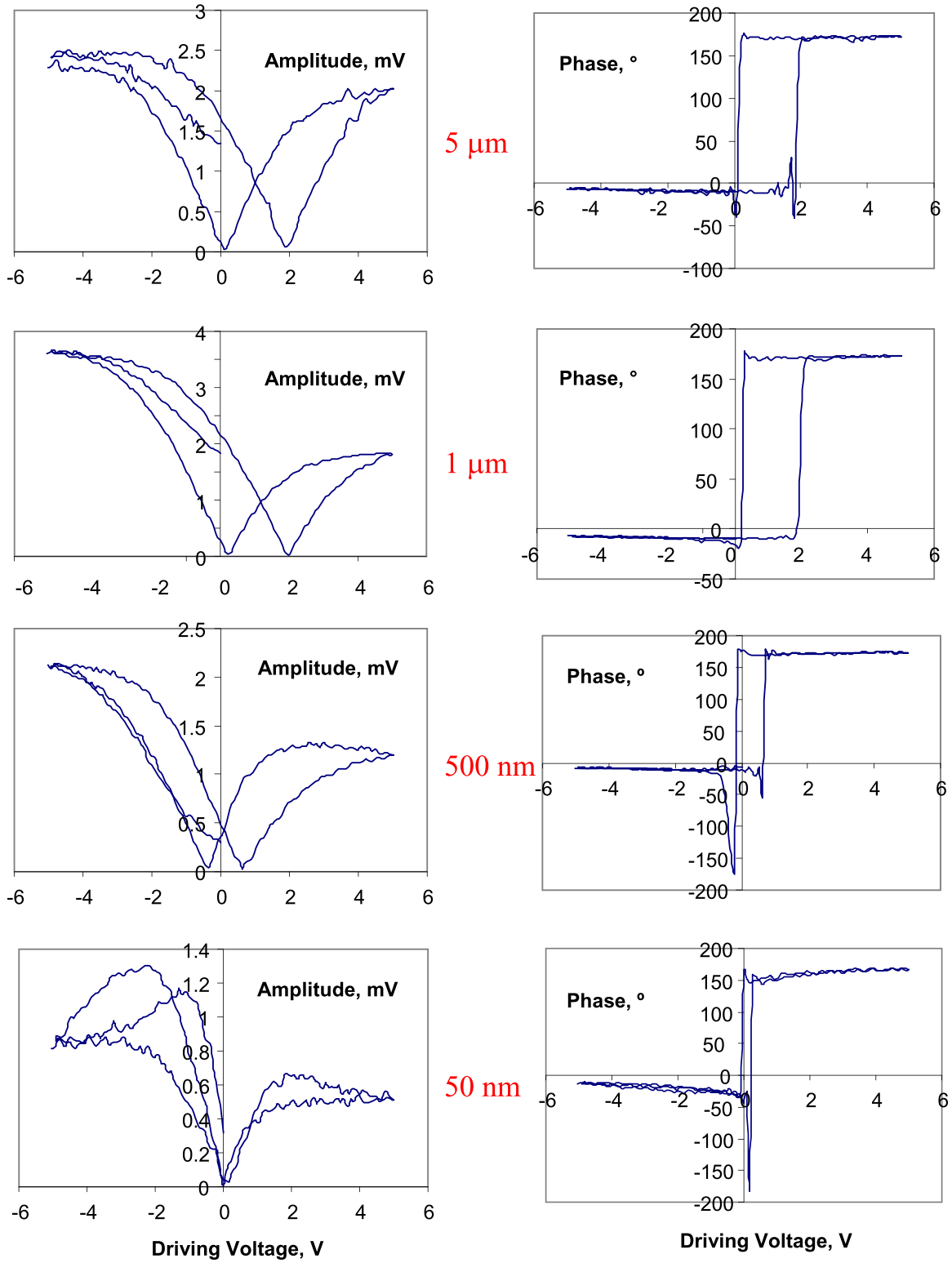

FIG. 3. PFM response amplitude (left) and phase (right) loops of PZT films with micro- and nanometrically sized top electrodes (5 μm, 1 μm, 500 nm, 50 nm from top to bottom).

A. Basic physical assumptions and calculation details

To calculate the spatial distribution of the electric field z-component $E_3(\rho, z)$ produced by the charged PFM tip in contact with top electrode on a ferroelectric film with the spontaneous polarization $P_3(\rho, z)$, where $\rho = \sqrt{x^2 + y^2}$ is the polar radius, z is the polar axis, it was assumed that (a) $P_3(\rho, z)$ is directed along the polar z-axis; (b) the film is dielectrically isotropic in transverse directions, i.e., permittivities $\varepsilon_{11} = \varepsilon_{22}$ and $\varepsilon_{33} \neq \varepsilon_{11,22}$; (c) film material can be regarded dielectrically uniform and elastically isotropic.

Using effective point charge approach,[17] PFM tip-electrode system under applied voltage V is modeled by: (a) a point charge $Q = 2\pi\varepsilon_0\varepsilon_e R_0 V(\kappa + \varepsilon_e)/\kappa$ located at the distance

$d = \varepsilon_e R_0/\kappa$ for a rounded tip-electrode with the radius R_0, where ε_e is the ambient dielectric constant; $\kappa = \sqrt{\varepsilon_{11}\varepsilon_{33}}$ is the effective dielectric constant determined by the dielectric permittivity in z-direction, (b) a point charge $Q = 4\varepsilon_0(\varepsilon_e + \kappa)R_0V$ located at the distance $d = 2R_0/\pi$ for a flattened electrode represented by a disk of radius R_0 in contact with the sample surface.[27] Vertical surface displacement below the tip-electrode was calculated in the decoupling approximation.

B. Coercive voltage size effect

In the continuous media approximation, both polarization and its second derivative are small in the close vicinity of the domain wall.[18] Under the typical condition of thin domain walls, a thermodynamically stable domain wall $\rho(z)$ can be estimated as the coercive point, i.e., under the condition $E_3(\rho, z) = E_c$, where the static coercive field E_c is determined from LGD equation with the coefficients renormalized by the finite size effects, screening conditions and elastic strains in thin films.[18]

From the algebraic equation of domain nucleation $E_3(\rho, z) = E_c$, the local approach allows us to estimate the functional dependence of the coercive voltage V_c on the ratio of the effective distance d determined by the tip-electrode radius R_0 to the film thickness h as[18]

$$V_c^{loc}(\rho, z) = E_c\left(\int_0^\infty dk J_0(k\rho)\cdot\frac{\cosh\left(k\,(h-z)/\gamma\right)}{\sinh(k\,h/\gamma)}\frac{kd}{\gamma}\exp(-kd)\right)^{-1}$$
$$\equiv E_c h\left(\int_0^\infty dq J_0\left(q\frac{\gamma\rho}{h}\right)\cdot\frac{\cosh\left(q\,(1-z/h)\right)}{\sinh(q)}q\xi\exp(-q\xi)\right)^{-1}, \quad (1)$$

where $J_0(k\rho)$ is the Bessel function of zero order, $\xi = \gamma d/h$ is the dimensionless effective tip-electrode size, and $\gamma = \sqrt{\varepsilon_{33}/\varepsilon_{11}}$ is the dielectric anisotropy factor.

Analytical expression derived at $\rho = 0$: $V_c^{loc}(0, z) = \frac{4E_c h}{\xi}\left(\mu\left(1,\, 1-\frac{z}{2h}+\frac{\xi}{2}\right)+\mu\left(1,\, 1+\frac{z}{2h}+\frac{\xi}{2}\right)\right)^{-1}$. Here, $\gamma_P(n, z)$ is polygamma function, the nth logarithmic derivative of the gamma function. Dependences of $V_c^{loc}(z)/hE_c$ on ξ are shown in Figure 3(a) for different $z/h = 0, 0.1, 0.2, 0.3, 0.5, 1$. As is obvious, ξ value determines the scale of size effect, which is noticeable at $\xi \le 10$. Dependences $V_c^{loc}(z)$ on ξ are pronouncedly non-monotonic in the range $0.1 < z/h < 0.3$ and $0.01 < \xi < 1$. Note that similar dependence for $V_c^{loc}(z)$, we obtain not only in the net LGD approach, but under self-consistent considering continuous lattice potential and domain walls diffuseness.[29]

The effective electric field is determined from the condition $\langle E_3(\rho, z)\rangle = E_c$, where $\langle E_3(\rho, z)\rangle$ is averaged over the semi-ellipsoidal domain with length l and the radius r. It was calculated that due to a high surface energy, the domain nuclei of radius r and length l has prolate semi-ellipsoidal shape.[30,31] The nuclei length is proportional to the effective PFM response depth γd, the radius $r \ll l$. Thus, in order to estimate effective coercive voltage one should average $V_c^{loc}(\rho, z)$ over the domain volume, which in result is proportional to the PFM response penetration depth $\sim\gamma d$, namely,

$$\langle V_c^{loc}(\rho, z)\rangle = \frac{1}{\pi r^2 l}\int_0^l dz\int_0^r \rho d\rho V_c^{loc}(\rho, z)$$
$$\sim \frac{1}{\gamma d}\int_0^{\gamma d} dz V_c^{loc}(0, z). \quad (2)$$

When the domain length value approaches the film thickness one should put $l = h$, in Eq. (2). In this case, $\langle V_c(z, \rho)\rangle \approx hE_c$ is independent on the tip-electrode effective size. Thus, it is reasonable to normalize $\langle V_c(z, \rho)\rangle$ on the value hE_c. The dependence $\langle V_c^{loc}(\rho, z)\rangle/hE_c$ on the parameter $\boldsymbol{\xi}$ is presented in Figure 3(b).

We assumed that the effective coercive voltage $\langle V_c^{loc}(\rho, z)\rangle$ given by Eq. (2) is registered experimentally in agreement with Landauer conception.[32]

IV. DISCUSSION

In correspondence with the results of theoretical consideration (see formula (1) and Fig. 4(a)), the significant difference in behaviour of V_c^{loc} values for different z/h becomes apparent when under decreasing the electrode lateral size and constant film thickness the value of ξ approaches to 1. The main change of $\langle V_c^{loc}(\rho, z)\rangle$ value also takes place in the vicinity of $\xi \approx 1$ (Fig. 4(b)).

The experimental electrode lateral size dependences of voltages V_{tc}^{+} and V_{tc}^{-} and amplitudes A_m^{+} and A_m^{-} derived from PFM response loops are presented in Figure 5.

The main change of V_{tc}^{+} and V_{tc}^{-} (Fig. 5(a)) is observed when the electrode lateral size decreases less than the film thickness. For the characteristic values of near morphotropic PZT ceramic compositions ($x = 0.52$), $\varepsilon_{11}{}^{T} \approx 1180$, $\varepsilon_{11}{}^{S} \approx 612$, and $\varepsilon_{33}{}^{T} \approx 730$, $\varepsilon_{33}{}^{S} \approx 399$ (Ref. 33) dielectric anisotropy factor $\gamma = (\varepsilon_{33}/\varepsilon_{11})^{1/2} \approx 0.8$ that under $d/h \approx 1$ corresponds to $\xi = \gamma d/h \approx 1$.

The comparison of the theoretical $\langle V_c^{loc}(\rho, z)\rangle(\xi)$ (Fig. 4(b)) and experimental $V_{tc}^{+/-}$ electrode size dependences (Fig. 5(a)) demonstrates that the behaviour of $\langle V_c^{loc}(\rho, z)\rangle$ corresponds to $V_{tc}^{+/-}$ behaviour registered experimentally. In fact, when the top electrode lateral size value is decreasing and approaching to h but the inequality $\xi > 1$ is still valid,

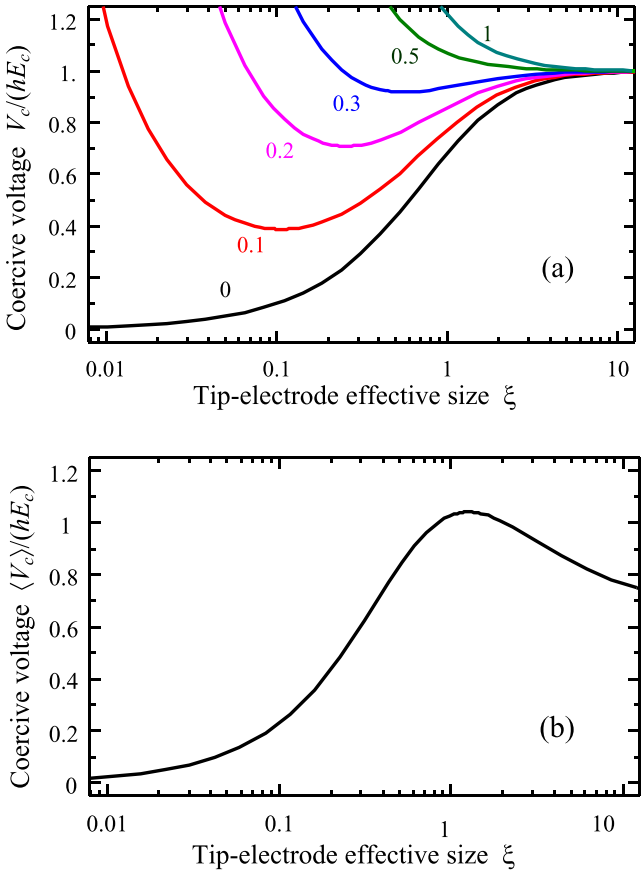

FIG. 4. (a) Local coercive voltages $\frac{V_c^{loc}(0,z)}{E_c h}$ vs. tip-electrode dimensionless size ξ for different $z/h = 0$, 0.1, 0.2, 0.3, 0.5, 1 (numbers near the curves). (b) Effective coercive voltage, i.e., $V_c^{loc}(\rho,z)$ averaged over the PFM response volume $\sim(\gamma d)^3$ as $\langle V_c^{loc}(\rho,z)\rangle = \frac{1}{\pi r^2 l}\int_0^l dz \int_0^r \rho d\rho V_c^{loc}(\rho,z) \sim \frac{1}{\gamma d}\int_0^{\gamma d} dz V_c^{loc}(0,z)$.

$\langle V_c^{loc}(\rho,z)\rangle$, $V_{tc}^{+/-}$ values are increasing and have a broad maximum just higher $\xi \approx 1$ and when $\xi < 1$, these values decrease with diminishing the top electrode lateral size. So, the theoretical and experimental electrode size dependences of coercive tip voltages are in a good agreement.

As for the observed behaviour of A_m^+ and A_m^- amplitudes (Fig. 5(b)), it should be considered allowing for the increase of damping due to the decrease of the ratio of area of directly excited film zone, which is mainly located under the top electrode, to the area of relaxation zone, which surrounded this electrode, under transition from plane-plane to point-plane electrode configuration.

It is worth noting that PFM response amplitude depends on the crystallographic orientation of the grains[34] and the dependence of the effective piezoelectric coefficient magnitude on the applied field direction was discussed in a number of publications.[35–37] In a real film, this problem is connected with the influence of domain pattern on the effective piezoelectric response.[33] Thus, for epitaxial PZT film with *c*/*a*/*c* domain structure,[38,39] the observed spatial variations of the piezoelectric response amplitude were explained by a local movement of ferroelastic 90°-*a*-domains and "spike-type" peaks of response amplitude near the coercive voltages were attributed to "ferroelastic 90°-*a*-domain switching to a *c*-domain."[40] At that point, in those studies together with apparent changes of an effective piezoelectric coefficient magnitude only rather small variations of coercive voltages were registered depending on domain pattern. This evidences the validity of considering the observed top electrode size effect regardless of the influence of domain structure for the examined films with preferable orientation.

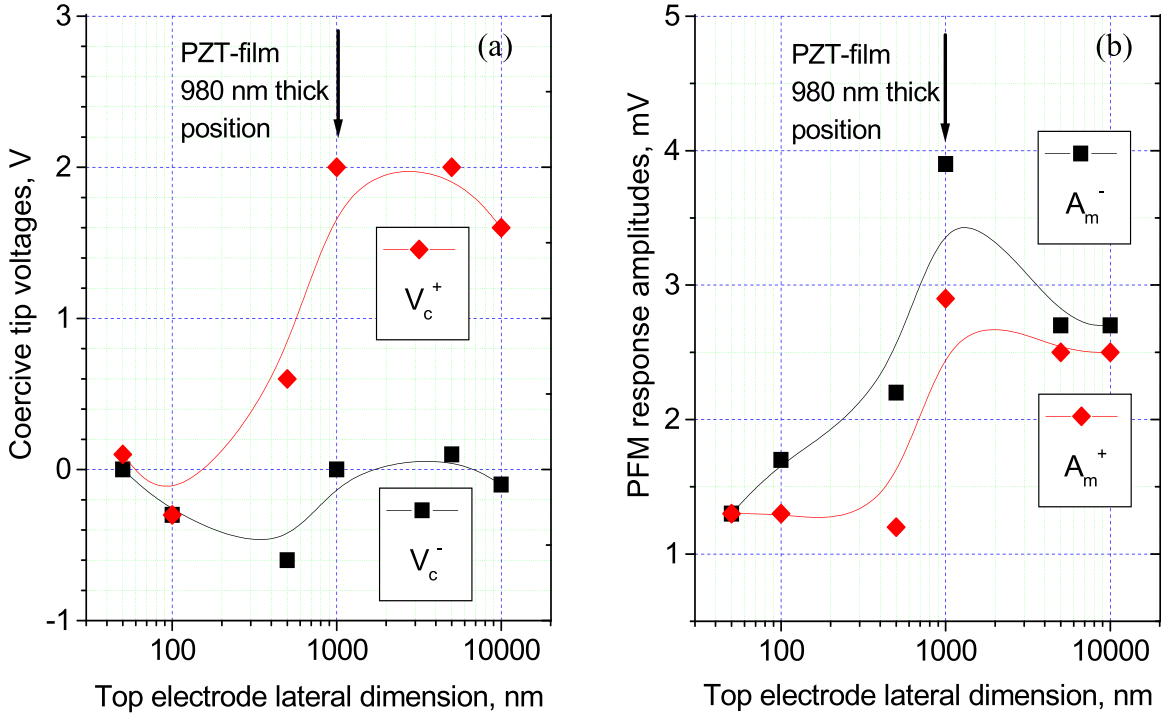

FIG. 5. Electrode size dependence of coercive voltages V_c^+ and V_c^- (a) and amplitudes A_m^+ and A_m^- (b) for positive (index "+") and negative (index "−") branches of PFM response loop. The points are experimental data and the lines are obtained by B-spline smoothing.

V. SUMMARY AND CONCLUSION

The Pt/PZT/Pt/TiO_x/SiO_2/Si-substrate structure with-$\approx$1 μm thick PZT-film deposited by RF magnetron sputtering and the set of evaporated top Pt (50 nm thick) electrodes with lateral size from 50 nm to 10 μm was examined with special emphasis on the effects of top electrode size in PFM response hysteresis loops.

The results of experimental studies display the transition-like behaviour of PFM amplitude and coercive tip voltage when the top electrode lateral size approaches to the film thickness.

The observed behaviour of coercive tip voltage around the critical value of effective electrode size was interpreted in the framework of the model based on Landau-Ginzburg-Devonshire theory combined with the decoupling approximation taking into account the nonlinear electric field dependence of the ferroelectric polarization and dielectric permittivity.

The theoretical studies should be extended to more complex consideration of the top electrode size effect taking into account polar anisotropy and domain structure, mechanical losses and measurement conditions, which influence the shape and volume of polarization reversal region that is reflected in PFM response hysteresis loops shape.

ACKNOWLEDGMENTS

N.V.M. and S.L.B. gratefully acknowledge the financial support of the University of Valenciennes.

[1]J. F. Scott, *Ferroelectrics Review* (Gordon and Breach Science, 1998), Vol. 1.
[2]J. F. Scott, *Ferroelectric Memories*, Springer Series in Advanced Microelectronics (Springer-Verlag, Berlin, 2000).
[3]A. L. Kholkin, Ch. Wütchrich, D. V. Taylor, and N. Setter, Rev. Sci. Instrum. **67**, 1935 (1996).
[4]P. Gerber, A. Roelofs, C. Kügeler, U. Böttger, and R. Waser, J. Appl. Phys. **96**(5), 2800 (2004).
[5]D. Fu, H. Suzuki, T. Ogawa, and K. Ishikawa, Appl. Phys. Lett. **80**, 3572 (2002).
[6]*Nanoscale Characterisation of Ferroelectric Materials*, 1st ed., edited by M. Alexe and A. Gruverman (Springer, Berlin, 2004).
[7]M. Alexe, J. F. Scott, C. Curran, N. D. Zakharov, D. Hesse, and A. Pignolet, Appl. Phys. Lett. **73**, 1592 (1998).
[8]M. Alexe, A. Gruverman, C. Harnagea, N. D. Zakharov, A. Pignolet, D. Hesse, and J. F. Scott, Appl. Phys. Lett. **75**, 1158 (1999).
[9]A. Gruverman, D. Wu, and J. F. Scott, Phys. Rev. Lett. **100**, 097601 (2008).
[10]A. Wu, P. M. Vilarinho, V. V. Shvartsman, G. Suchaneck, and A. L. Kholkin, Nanotechnology **16**, 2587 (2005).
[11]V. V. Shvartsman, A. Y. Emelyanov, A. L. Kholkin, and A. Safari, Appl. Phys. Lett. **81**, 117–119 (2002).
[12]B. J. Rodriguez, S. Jesse, A. P. Baddorf, Y. H. Chu, T. Zhao, R. Ramesh, E. A. Eliseev, A. N. Morozovska, and S. V. Kalinin, Nanotechnology **18**, 405701 (2007).
[13]V. V. Shvartsman, A. L. Kholkin, M. Tyunina, and J. Levoska, Appl. Phys. Lett. **86**, 222907 (2005).
[14]V. V. Shvartsman and A. L. Kholkin, J. Appl. Phys. **101**, 064108 (2007).
[15]A. Gruverman, B. J. Rodriguez, A. I. Kingon, R. J. Nemanich, A. K. Tagantsev, J. S. Cross, and M. Tsukada, Appl. Phys. Lett. **83**, 728 (2003).
[16]A. Gruverman, B. J. Rodriguez, C. Dehoff, J. D. Waldrep, A. I. Kingon, R. J. Nemanich, and J. S. Cross, Appl. Phys. Lett. **87**, 082902 (2005).
[17]L. Tian, A. Vasudevarao, A. N. Morozovska, E. A. Eliseev, S. V. Kalinin, and V. Gopalan, J. Appl. Phys. **104**, 074110 (2008).
[18]A. N. Morozovska, E. A. Eliseev, S. L. Bravina, and S. V. Kalinin, J. Appl. Phys. **110**, 052011 (2011).
[19]S. Bravina, N. Morozovsky, E. Eliseev, A. Morozovska, J. Costecalde, C. Soyer, D. Remiens, and D. Deresmes, Proceedings of ISAF-PFM 2011, Vancouver, Canada, July 2011.
[20]G. Velu and D. Remiens, J. Eur. Ceram. Soc. **19**, 2005 (1999).
[21]T. Haccart, E. Cattan, and D. Remiens, Semicond. Phys., Quantum Electron. Optoelectron. **5**, 78 (2002).
[22]S. L. Bravina, E. A. Eliseev, N. V. Morozovsky, D. Remiens, C. Soyer, and A. Grosman, "Pyroactive PZT-film/Si, PZT-film/Por-Si/Si and P(VDF/TrFE)-film/Si structures for integrated IR-sensorics" in *Pyroelectric Materials and Sensors* (Research Signpost, Kerala, India, 2007), Chap. 1, pp. 1–23.
[23]S. L. Bravina, N. V. Morozovsky, D. Remiens, and C. Soyer, Ferroelectrics **353**, 193 (2007).
[24]A. L. Kholkin, V. V. Shvartsman, A. Yu. Emelyanov *et al.*, Appl. Phys. Lett. **82**, 2127 (2003).
[25]*Scanning Probe Microscopy—Electrical and Electromechanical Phenomena at the Nanoscale*, edited by S. Kalinin and A. Gruverman (Springer-Verlag, 2006).
[26]D. A. Scrymgeour, V. Gopalan, A. Itagi, A. Saxena, and P. J. Swart, Phys. Rev. B **71**, 184110 (2005).
[27]F. Felten, G. A. Schneider, J. Muñoz Saldaña, and S. V. Kalinin, J. Appl. Phys. **96**, 563–568 (2004).
[28]A. N. Morozovska, E. A. Eliseev, and S. V. Kalinin, Appl. Phys. Lett. **89**, 192901 (2006).
[29]E. V. Burtsev and S. P. Chervonobrodov, Ferroelectrics **45**, 97–106 (1982).
[30]I. Bdikin, A. Kholkin, A. N. Morozovska, S. V. Svechnikov, S.-H. Kim, and S. V. Kalinin, Appl. Phys. Lett. **92**, 182909 (2008).
[31]A. N. Morozovska, S. V. Svechnikov, E. A. Eliseev, S. Jesse, B. J. Rodriguez, and S. V. Kalinin, J. Appl. Phys. **102**, 114108 (2007).
[32]R. Landauer, J. Appl. Phys. **28**, 227 (1957).
[33]B. Jaffe, W. R. Cook, and H. Jaffe, *Piezoelectric Ceramics* (Academic, London, 1971).
[34]C. Harnagea, A. Pignolet, M. Alexe, and D. Hesse, Integr. Ferrelectr. **44**, 113 (2002).
[35]X. Du, U. Belegundu, and K. Uchino, Jpn. J. Appl. Phys., Part 1 **36**, 5580 (1997).
[36]C. Harnagea, A. Pignolet, M. Alexe, D. Hesse, and U. Gösele, Appl. Phys. A: Mater. Sci. Process. **70**, 261 (2000).
[37]C. Harnagea and A. Pignolet, *Current Issues on Multidisciplinary Microscopy Research and Education* (FORMATEX, 2004), p. 156.
[38]A. L. Roitburd, Phys. Status Solidi A **37**, 329 (1976).
[39]A. L. Roytburd, S. P. Alpay, L. A. Bendersky, V. Nagarajan, and R. Ramesh, J. Appl. Phys. **89**, 553 (2001).
[40]G. Le Rhun, I. Vrejoiu, and M. Alexe, Appl. Phys. Lett. **90**, 012908 (2007).